




## Atomistic insights into the impact of charge balancing cations on the structure and properties of aluminosilicate glasses

Achraf Atila <sup>1,\*</sup> El Mehdi Ghardi <sup>2</sup> Said Ouaskit,<sup>2</sup> and Abdellatif Hasnaoui <sup>3,†</sup>

<sup>1</sup>*Materials Science and Engineering, Institute I, Friedrich-Alexander-Universität Erlangen-Nürnberg (FAU), Martensstr. 5, Erlangen 91058, Germany*

<sup>2</sup>*Laboratoire de Physique de la Matière Condensée, Faculté des Sciences Ben M'sik, Université Hassan II de Casablanca, B.P 7955, Av Driss El Harti, Sidi Othmane, Casablanca, Maroc*

<sup>3</sup>*LS3M, Faculté Polydisciplinaire Khouribga, Sultan Moulay Slimane University, B.P 145, 25000 Khouribga, Morocco*



(Received 30 July 2019; revised manuscript received 30 September 2019; published 31 October 2019)

Ternary aluminosilicate glasses are of great interest in glass and earth sciences. The structural role of the non-network cations is not fully understood until now. Understanding the structural effect of the non-network cations is necessary for explaining their impact on the macroscopic properties of aluminosilicate glasses. In this work, we use molecular dynamics to investigate physical properties of a series of charge balanced aluminosilicate glasses. Elastic properties and the glass transition temperature were calculated. Our results are in accordance with the experimental data found in the literature. We found that elastic moduli increase with the charge balancing cations field strength (FS), while the glass transition temperature is negatively correlated to FS. The effect of the charge balancing cations field strength on the calculated properties is discussed and explained using the change in the structural properties, energetic environment of atoms, and two-body excess entropy. This allows us to get an overview of the effect of cations nature on the properties of the glass.

DOI: [10.1103/PhysRevB.100.144109](https://doi.org/10.1103/PhysRevB.100.144109)

### I. INTRODUCTION

Elasticity is a material property used in understanding various physical properties in glassy materials, such as thermal shock resistance or fracture toughness. Basically, if a material is loaded with a certain force value, this causes a displacement of atoms which results in a response in the form of deformation, which gives a general view of the mechanical behavior of the material [1,2].

Oxide glasses have been used in several applications, starting from windows to screens for electronic devices and optical fibers [3]. In fact, it is always desirable to get high elastic moduli, e.g., to produce thinner and stiffer substrates for thin film electronics or screens for smart phones. The mechanical behavior of oxide glasses depends strongly on the content and type of non-network cations. The presence of an intermediate oxide such as alumina also affects the mechanical response of the glass. Indeed, the type of network former such as silicates [4–6], borates [7,8], phosphates [9,10], or mixed formers glasses [11,12] plays a critical role in the mechanical behavior of the glass. Thus, there is always a way to improve mechanical properties of oxide glasses through topological engineering by designing specific glass compositions for some target applications. For this purpose, we need a deep understanding of the current knowledge of the relationship between structure, mechanical properties, composition, and other physical/chemical properties of the glasses.

An interesting type of oxide glasses is the aluminosilicates. Their relevance is mainly due to their good mechanical and

thermal properties, without neglecting the abundance of the glass elements in the earth mental [2]. This family of glasses is often used in the development of new glasses, with superior properties to meet the needs for various industrial and technological applications [13,14]. Aluminosilicate glasses are also used as glass ceramics, especially for low thermal expansion materials. These later materials are usually based on the lithium aluminosilicate glass system. High strength glass ceramics can also be prepared based on the magnesium aluminosilicate [14]. Numerous studies on aluminosilicate glasses modified by different types of cations (e.g., alkali and/or alkaline earth, rare-earth metals) were performed in order to get a better understanding of the relationship between composition and properties [13,15,16].

The distribution of aluminum species in aluminosilicate glasses depends on the type and content of modifiers added to the glass network and more precisely on the concentration ratio  $[X_{2/n}^{n+}O]/[Al_2O_3]$  (where  $X$  stands for the modifier). Thus, the distribution of Al tetrahedra  $Al^{[4]}$ , five-coordinated  $Al^{[5]}$ , and octahedra  $Al^{[6]}$  will depend on that ratio. Indeed, when the concentration of modifiers  $X_{2/n}^{n+}O$  is found in excess or equal to the alumina content,  $Al^{3+}$  ions are essentially present in four-coordinated configuration  $Al^{[4]}$  and their negative charges are compensated by  $X_{2/n}^{n+}$  cations [17]. In the metaluminous join, where  $[X_{2/n}^{n+}O]/[Al_2O_3] = 1$ , all  $X_{2/n}^{n+}O$  ions are supposed to compensate the charges generated by  $Al^{[4]}$  tetrahedra. These glasses are supposed to be completely polymerized and can no longer have nonbridging oxygens (NBOs). In the peraluminous region where  $[X_{2/n}^{n+}O]/[Al_2O_3] < 1$ , the glasses have an excess of modifiers compared to alumina.  $Al^{3+}$  ions are compensated by the modifiers and are predominantly in

\*achraf.atila@fau.de

†hasnaoui59@hotmail.com

four-coordinated configuration Al<sup>[4]</sup>. The excess of aluminum atoms is inserted into the vitreous network in five-coordinated Al<sup>[5]</sup> and six-coordinated Al<sup>[6]</sup>.

Indeed, the nature and composition of the glass affect the formation of highly coordinated species. Mg<sup>2+</sup> and Zn<sup>2+</sup> are known to have high field strength which promotes the formation of Al<sup>[5]</sup> as shown by Kelsey *et al.* [18]. Moreover, using experiments Allwardt *et al.* studied aluminosilicate glasses containing Na<sup>+</sup>, K<sup>+</sup>, and Ca<sup>2+</sup> and showed that increasing cation field strength increases the average Al coordination number [19]; this behavior has also been observed in the experimental study of Kelesey *et al.* [20].

Until now, the atomic scale mechanisms of the effect of charge balancing cations on the structural and physical properties in aluminosilicate glasses has not been studied in detail. Herein, we present atomistic simulations to highlight in details the effect of the charge balancing cations field strength on the thermodynamic and mechanical properties and its structural origins in the aluminosilicate glasses.

We investigate the physical properties of a series of charge balanced aluminosilicate glasses. We aim to clarify the role of different cations in altering the structure and physical properties of the aluminosilicate glasses. The concentration of the charge balancing oxides was set to be equal to that of the alumina  $[X_{n/2}^{n+}O]/[Al_2O_3] = 1$  ( $X = \text{Li, Na, K, Mg, Ca, Sr, Ba, and Zn}$ ). This is assumed to produce a fully connected three-dimensional glass network in which the major blocks are the randomly distributed aluminum and silicon tetrahedra and the negative charge of Al<sup>[4]</sup> tetrahedra is supposed to be compensated by the charge balancing cations. Even if our glasses contain either mono- or divalent alkali, alkaline earth, or Zn cations, they are expected to play similar roles in the aluminosilicate glass network, as charge balancers for Al<sup>[ $n$ ]</sup>, ( $n = 4, 5, 6$ ) polyhedra. However, due to the difference in the size of charge balancing cations, the ability to charge balance will be different as the same charge is distributed over a larger area for larger cations. In the present work, this difference will be quantified as the field strength (FS).

Molecular dynamics (MD) simulations, which is an effective method to help investigating and understanding the atomic scale behavior of materials and has been applied in studying metallic and oxide glasses [21–25] and mechanical behavior of nanocrystalline materials [26–28]. Molecular dynamics simulations allowed us to identify the origins of different charge balancing cations on the measured properties at the atomic scale.

We calculated the glass transition temperature, elastic moduli and correlated them to structural modifications imposed by each cation. The influence of charge balancing cations is highlighted via a variation of measured properties as a function of the charge balancing cations field strength.

This paper is organized as follows. In Sec. II, we give a description of the simulation procedure, the interatomic potential used in our simulations, and we provide a brief description of the different tools used to analyze the structure and compute the different properties. In Sec. III, we present the results by dividing them into three parts: The glass transition temperature, mechanical properties, and structural properties. Section IV contains a discussion of the results which correlates between structural change, modifier cations

field strength, and mechanical properties. Concluding remarks are given in Sec. V.

## II. COMPUTATIONAL DETAILS AND METHODOLOGY

### A. Interatomic potential model

The accuracy of molecular dynamics results is strongly influenced by the choice of the interatomic potential function that describes interactions between atoms. In this context, the rigid ionic model with partial charges was used for calculating the forces that act on atoms and to simulate the ionocovalent nature of bonding in modified aluminosilicate glass systems. In this model, the particles are treated as charge points interacting via Coulomb forces with a short-range potential describing interaction between pairs of atoms. We employed the well-established potential developed by Pedone *et al.* [29]. The functional form of the potential is given by:

$$U(r_{ij}) = \frac{z_i z_j e^2}{r} + D_{ij} [1 - e^{-a_{ij}(r-r_0)^2} - 1] + \frac{C_{ij}}{r^{12}} \quad (1)$$

where  $i$  and  $j$  are atoms (Si, O, Al, Li, Na, K, Ca, Mg, Sr, Ba, or Zn),  $r$  is the distance between atoms  $i$  and  $j$ ,  $z_i$  and  $z_j$  are the effective charges of the atoms  $i$  and  $j$ .  $D_{ij}$ ,  $a_{ij}$ ,  $r_0$ , and  $C_{ij}$  are potential parameters. The first term in Eq. (1) describes the long-range electrostatic interaction between atoms, the second one is a short-range Morse function which is usually used in modeling bonded interactions in covalent systems, and the last term represents a repulsive contribution, necessary to model the interaction at high temperature and pressure [29]. This potential gives a realistic agreement with available experimental data as mentioned in the literature [6,29–32]. Potential parameters and partial charges are given in Ref. [29]. All simulations were performed using the large-scale atomic/molecular massively parallel simulator LAMMPS [33] while all visualizations are made by the aid of OVITO [34].

### B. Glass preparation and composition details

We simulated eight charge balanced aluminosilicate glasses  $(X_{n/2}^{n+}O - Al_2O_3) - 0.5(SiO_2)$  where  $X$  stands for Li, Na, K, Mg, Ca, Sr, Ba, and Zn, using classical molecular dynamics. Table I gives details about each system label, density, glass transition temperature and the field strength which is defined as the ratio of the formal charge  $z$  divided by the

TABLE I. Details for each composition: Density ( $\rho$ ) after stress relaxation, field strength (FS), and the glass transition temperature ( $T_{\text{gsim}}$ ) from our simulations. Experiment values from Ref. [2] are given between parenthesis.

Glass	$\rho$ (g/cm <sup>3</sup> )	FS ( $\text{\AA}^{-2}$ )	$T_{\text{gsim}} \pm 30$ (K)
LiAS	2.554 (2.431)	1.49	1283 (922)
NaAS	2.617 (2.494)	0.69	1432 (1074)
KAS	2.562 (2.463)	0.39	1526 (1193)
MgAS	2.804 (2.678)	3.12	1376 (1082)
CaAS	2.810 (2.960)	1.51	1398 (1131)
SrAS	3.144 (3.021)	1.13	1440 (1152)
BaAS	3.448 (3.300)	0.89	1423 (1149)
ZnAS	3.235 (3.091)	3.12	1365 (1022)

square of the effective cation radius  $r$ ,  $Z/r^2$ ; experimental data [2] are given between parenthesis for comparison. All systems consist of approximately 4200 atoms placed randomly in a cubic simulation box ensuring that there is no unrealistic overlap between atoms. An integration time step of 1 fs was used with periodic boundary conditions (PBC) applied in all directions to avoid edge effects on the systems. Long-range interactions were evaluated by Ewald summation method, with a real space cutoff of 12.0 Å and precision of  $10^{-6}$ . The short-range interaction cutoff distance was chosen to be 5.5 Å [29]. First, we equilibrated the systems in NVT at high temperature ( $T = 5000$  K) for 500 ps, which is enough to bring our systems to the liquid state in the context of the used force field. This step is needed to obtain an equilibrated liquid as well as to ensure that each system loses memory of its initial configuration. The second step is the linear quenching from the liquid temperature ( $T = 5000$  K) to room temperature ( $T = 300$  K) with a cooling rate of 1 K/ps in NVT. However, cooling in NVT gives glasses containing an amount of stress which needs to be released; for that the system was equilibrated at room temperature and zero pressure in NPT for 1 ns to make the systems stress free and another supplementary 100 ps in the NVT ensemble for statistical averaging over 100 configurations each separated by 1 ps. Temperature and pressure controls were affected using Nosé-Hoover thermostat and barostat. As a matter of fact, cooling rates used in molecular dynamics are much higher than those used in experiments due to the intrinsic incapability of molecular dynamics to use very low cooling rates. The values of the cooling rate used in the present simulations are usually used in making glasses in MD simulations, and changing these values over a magnitude of order does not affect considerably the physical properties and the short-range structure of the glassy state [35,36].

### C. Structural analysis and properties calculation

#### 1. Radial distribution functions and coordination numbers

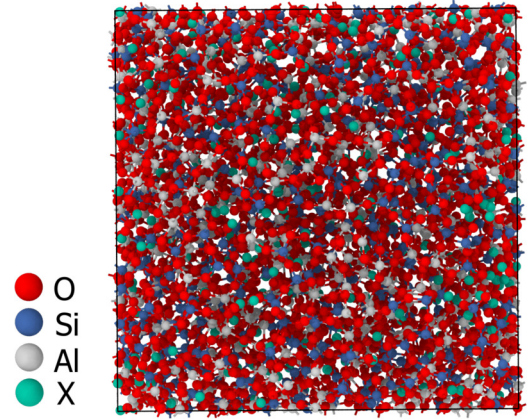
The radial distribution function (RDF) is used to describe the local atomic structure of the systems [37]. The RDF, which is defined as the probability of finding an atom  $j$  away from atom  $i$ , is given by:

$$g_{ij}(r) = \frac{1}{4\pi r^2 \rho_j} \left[ \frac{dN_{ij}(r)}{dr} \right] \quad (2)$$

where  $i$ ,  $j$  are atoms and  $N_{ij}(r)$  stands for the average number of  $j$  atoms in the sphere centered on  $i$  atoms with a radius  $r$ . Otherwise, we can also get some insight into the ordering of the glasses by the determination of the coordination number  $N_{ij}$  in the first coordination shell. The coordination number  $N_{ij}$  is the number of  $j$  atoms around an atom  $i$  and it is calculated by integrating the RDF from zero up to first minimum  $r_{\min}$  delimiting the first neighboring shell,

$$N_{ij}(r_{\min}) = 4\pi \rho \int_0^{r_{\min}} g_{ij}(r) r^2 dr. \quad (3)$$

It is also worth mentioning that the values of  $N_{ij}$  are very sensitive to the choice of  $r_{\min}$ . This  $r_{\min}$  must be carefully determined for each pair function (Fig. 1).



X = Li, Na, K, Mg, Ca, Sr, Ba or Zn

FIG. 1. Representative snapshot of the atomic structure of the studied charge balanced aluminosilicate glasses.

#### 2. Angular distribution functions (ADF)

For further analysis of the glasses local structures we refer to the angular distribution functions (ADF). The ADF can be explained by the fact that each combination of three atoms can form a triangle [37]; it consists of finding those triangles and getting a measure of bond angles as

$$\theta_{ijk} = \arccos \left( \frac{r_{ij}^2 + r_{ik}^2 - r_{jk}^2}{2r_{ij}r_{ik}} \right) \quad (4)$$

$$P(\theta) = \frac{n}{N} \quad (5)$$

where  $r_{ij}$  corresponds to the distance between two atoms,  $n$  is the number of angles  $i-j-k$  at angles  $\theta$  within a sphere of radius  $r_{\min}$  as determined from the RDF, and  $N$  is the total number of  $i-j-k$  angles in the same sphere. In our study, the ADF is used to estimate the angle between inter- and intratetrahedral units of the systems and also to describe the local structure around the charge balancing cations.

#### 3. Atomic entropy fingerprint

In general, an accurate computation of the entropy is extremely costly. Thus, an expression that gives approximately the entropy is sufficient to show how different cations can affect the entropy of the glasses. This expression was derived from an expansion of the configurational entropy in terms of multibody correlation functions [38,39]. Equation (6) presents the two-body excess entropy which involves only the pair correlation function and accounts for about 90% of the configurational entropy [38–40].

$$S_2 = -2\pi \rho k_B \int_0^{r_m} [g(r) \ln g(r) - g(r) + 1] r^2 dr \quad (6)$$

This equation can also be extended to compute the entropy fingerprint for each particle  $i$  in the systems [41,42]

$$S_2^i = -2\pi \rho k_B \int_0^{r_m} [g_m^i(r) \ln g_m^i(r) - g_m^i(r) + 1] r^2 dr \quad (7)$$

where  $\rho$  is the system's density, and  $g_m^i(r)$  is the radial distribution function for the particle  $i$ . To obtain a continuous

and differentiable order parameter, the mollified version of the radial distribution function was computed as described in Ref. [39] and implemented in the LAMMPS code [33], it is given by

$$g_m^i(r) = \frac{1}{4\pi\rho r^2} \sum_j \frac{1}{\sqrt{2\pi\sigma^2}} e^{-(r-r_{ij})^2/(2\sigma^2)} \quad (8)$$

where  $j$  describes the neighbors of atom  $i$ ,  $r_{ij}$  is the distance between atoms  $i$  and  $j$ , and  $\sigma$  is a broadening parameter. We shall choose  $\sigma$  small enough to get  $g_m(r) \simeq g(r)$  and large enough to manage derivatives of atomic positions [39].

#### 4. Elastic properties calculation

To compute the elastic properties, the second derivative method was applied. This technique can be used to get the stiffness matrix as well as the compliance matrix. Using a single-point energy calculation the stiffness matrix elements are obtained by:

$$C_{ij} = \frac{1}{V} \frac{\partial^2 U}{\partial \varepsilon_\alpha \partial \varepsilon_\beta}. \quad (9)$$

In isotropic cubic materials, there exist only two independent parameters of the stiffness matrix ( $C_{11}$  and  $C_{44}$ ) [29]. In the Voigt convention, the bulk, shear, and Young moduli can be calculated from Eqs. (10)–(12) while the Poisson ratio is given by Eq. (13).

$$B_{\text{Voigt}} = \frac{1}{9}(C_{11} + C_{22} + C_{33} + 2(C_{12} + C_{13} + C_{23})) \quad (10)$$

$$G_{\text{Voigt}} = \frac{1}{15}(C_{11} + C_{22} + C_{33} + 3(C_{44} + C_{55} + C_{66}) - C_{12} - C_{13} - C_{23}) \quad (11)$$

$$E = \frac{9BG}{3B + G} \quad (12)$$

$$\nu = \frac{E}{2G} - 1 \quad (13)$$

The obtained mechanical properties reported in this paper were calculated using molecular statics through energy minimization at 0 K. The obtained glass structures at 300 K were subjected to a quench to 0 K by energy minimization using the conjugate gradient algorithm. The minimized structures were deformed in each of the six directions in both positive and negative deformations and the change in the stress tensor was measured.

### III. RESULTS

#### A. Elastic properties

Figure 2 depicts the variation of the elastic moduli from our simulations and experiments as a function of the cations field strength. As shown in this figure, the elastic moduli obtained by MD simulations are in realistic agreements with the experimental data measured by Brillouin light scattering (BLS) [2]. The elastic moduli are correlated positively with the charge balancing cations field strength, while the Poisson's ratio remains almost constant with a value around 0.25 for alkali aluminosilicate glasses and 0.27 for alkaline earth and Zn aluminosilicate glasses. The Young modulus ( $E$ ) increases as a function of the FS, which is also an indication of increasing bond strength in those glasses. This behavior has also been observed for the bulk ( $B$ ) and shear ( $G$ ) moduli. Moreover, for the present charge balanced aluminosilicate glasses, the Poisson's ratio  $\nu$  doesn't show a clear correlation as a function of the FS as seen in Fig. 2(d) and it is dependent on the type of charge balancing cation. Furthermore, the elements with very

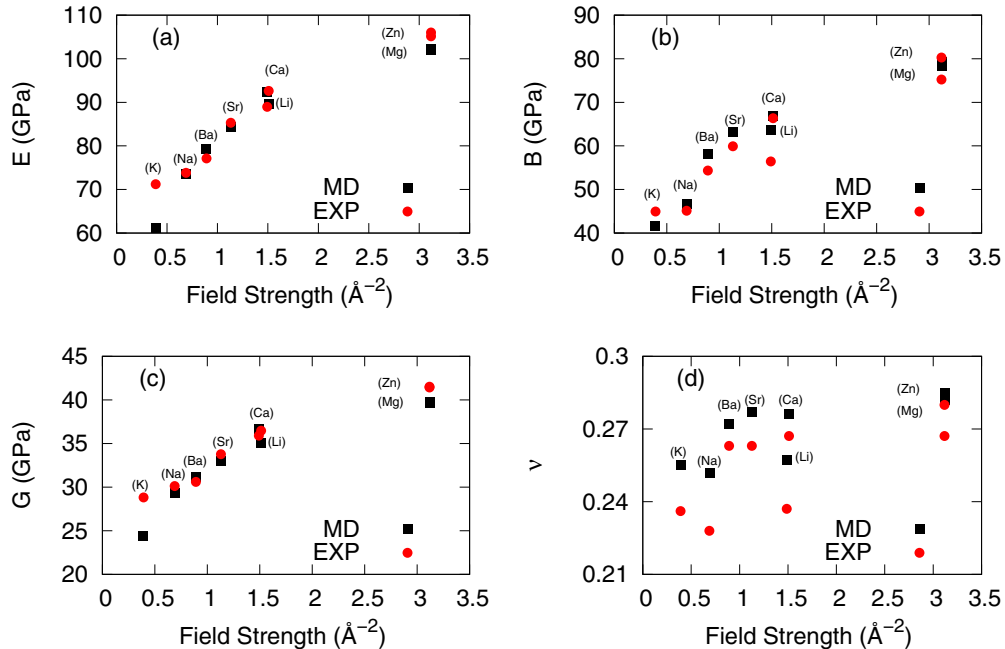


FIG. 2. (a) Young's modulus ( $E$ ), (b) bulk modulus ( $B$ ), (c) shear modulus ( $G$ ), and (d) Poisson's ratio as a function of the charge balancing cations field strength, compared with experimental values from Ref. [2].

TABLE II. Values of Young modulus (E), bulk modulus (B), shear modulus (G), and Poisson's ratio ( $\nu$ ) found in our simulations compared with experiments found in Ref. [2]; absolute errors are also given.

System		E (GPa)	B (GPa)	G (GPa)	$\nu$
LiAS	MD	92.36	63.57	36.71	0.257
	exp	88.90	56.40	35.90	0.237
	error (%)	3.892	12.713	2.256	8.439
NaAS	MD	73.51	46.59	29.33	0.252
	exp	73.90	45.20	30.10	0.228
	error (%)	0.527	3.075	2.558	8.051
KAS	MD	61.23	41.72	24.38	0.255
	exp	71.20	45	28.80	0.236
	error (%)	14.00	7.289	15.347	8.051
MgAS	MD	101.94	78.41	39.82	0.282
	exp	105.2	75.20	41.50	0.267
	error (%)	2.88	4.268	4.0482	5.617
CaAS	MD	89.67	66.89	35.12	0.276
	exp	92.60	66.30	36.50	0.267
	error (%)	3.164	0.890	3.781	3.371
SrAS	MD	84.24	63.21	32.96	0.277
	exp	85.30	59.90	33.80	0.263
	error (%)	1.243	5.526	2.485	5.323
BaAS	MD	79.41	58.22	31.2	0.272
	exp	77.20	54.40	30.60	0.263
	error (%)	1.023	7.022	1.961	3.422
ZnAS	MD	102.17	79.33	39.63	0.285
	exp	106.10	80.30	41.63	0.28
	error (%)	3.921	1.208	4.804	1.785

close values of the field strength have similar values of the elastic moduli. A summary of the calculated elastic properties and relative errors with respect to experimental data is given in Table II.

### B. Glass transition temperature

The glass transition temperature can be found by plotting the variation of some physical, chemical, or thermodynamic properties of the material such as volume  $[V(T)]$ , total energy  $E_t(T)$ , or enthalpy  $H(T)$  with respect to temperature [43,44] or using some mechanical properties such as fracture toughness [45]. The glass transition temperature is then obtained from the slope break between high- and low-temperature variations of that property versus temperature. Values reported here are those obtained using the total energy as a function of the temperature  $E_t(T)$  ( $E_t$  stands for total energy). Figure 3 plots  $T_g$  values as a function of FS obtained in the present simulations together with the experimental values. We observe from this figure a striking qualitative similarity between the MD and experimental results. However, we remark that the MD overestimates  $T_g$  values by 200 to 300 K compared to experiments. This is a well known behavior in MD simulations which is generally attributed to the very high cooling rates used in MD simulations [36]. Another effect may be linked to the fact that the interatomic potentials are not fitted to reproduce the behavior of the glass transition due to the complexity

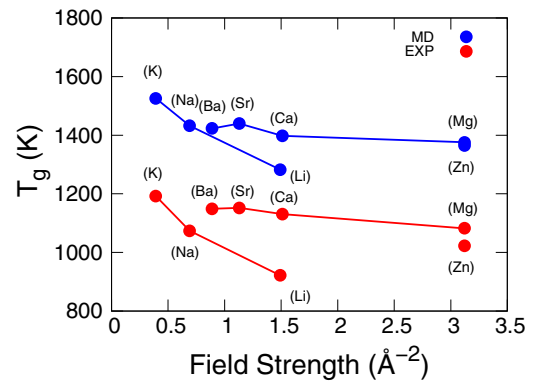


FIG. 3. Glass transition temperature as a function of cations field strength compared with experimental values found in Ref. [2].

of the phenomenon. The FS increases along the series  $K^+ < Na^+ < Li^+$  and  $Ba^{2+} < Sr^{2+} < Ca^{2+} < Mg^{2+}$  while FS of  $Zn^{2+}$  is equivalent to that of  $Mg^{2+}$ . We also observe from Fig. 3 that as the FS increases the glass transition temperature generally decreases for both alkali and alkaline earth systems, with a more pronounced decrease for alkali aluminosilicate glasses. The variation of  $T_g$  as a function of FS is found to follow,  $Li < Na < K$ , and  $Zn < Mg < Ca < Ba < Sr$ .

For the present glass systems, we notice that  $T_g$  depends on the FS of the non-network former cations, thus it depends directly on the radius of the charge balancing cations. Romano *et al.* [46] reported almost the same trends in the viscosity of  $XAlSi_3O_8$  melts in the region of  $T_g$ , where  $X$  stands for (Li, Na, K,  $Ca_{0.5}$ ,  $Mg_{0.5}$ ). It is also known that in aluminosilicate glasses  $T-O$  ( $T = Si$  or  $Al$ ) bonds are the strongest. The introduction of a modifier cation induces a perturbation to these bonds in a form of competition between Si, Al, and  $X$  atoms to form bonds with oxygens ( $X$  is the nonframework cation). Indeed, increasing the field strength of the modifying cations leads to an increase of the perturbation in the glass network and increases the probability of the nonframework cations to form bonds with oxygen atoms [47]. In addition, as illustrated in Fig. 3,  $T_g$  in CaAS glass is higher than that of MgAS glass; this correlates well with the fact that the radius of Mg cations is smaller than that of Ca cations. It is also observed from Figs. 2 and 3, that when the FS increases the elastic moduli (EM) increase while  $T_g$  decreases. This reveals a negative correlation of the EM with  $T_g$  for both alkali and alkaline earth aluminosilicate glasses.

### C. Structural properties

#### 1. Local environment of network formers

In the ternary aluminosilicate glasses, both Si and Al can attain different coordination numbers with oxygen, depending on the chemical composition, as well as on thermal and pressure histories of the glass [19,48]. Network-forming Si and Al cations coordinated with more than four and three oxygen anions, respectively, require a network modifier (e.g., alkali cations) to maintain charge neutrality.

In Fig. 4, we plotted the first peaks of Si-O and Al-O RDFs. We observe that the first peaks of the Si-O and Al-O RDFs show maxima at distances around 1.61 Å and 1.73 Å, respectively, in accordance with the data reported in the literature

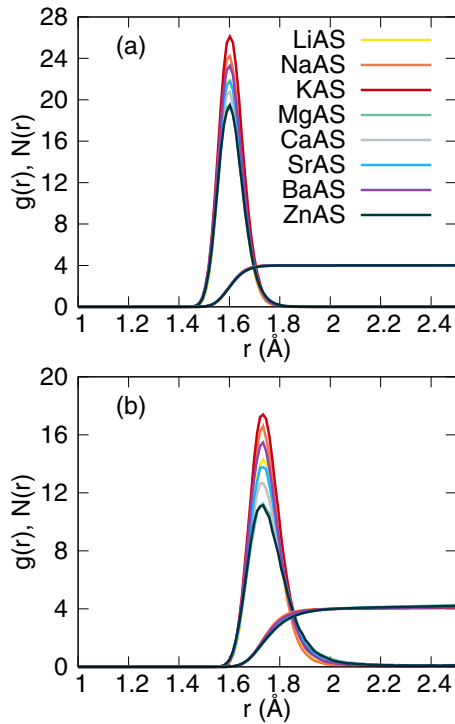


FIG. 4. RDFs and the cumulative coordination function in the obtained glasses at 300 K. (a) Si-O and (b) Al-O.

[13,15,21,49]. Additionally, we see that the first peak position, which represents the mean distance between each pair, is not affected by the type of the charge balancing cations. However, it is systematically observed that if the cations field strength increases the intensity of the first peak decreases.

By integrating the partial radial distribution functions to a specific cutoff value defined as the first minimum of each RDF, we can obtain the averaged coordination numbers of both network formers. This minimum is found to be 2.1 Å and 2.3 Å for Si-O and Al-O, respectively. The results show that both network formers have a coordination around 4.0 for Si atoms and 4.1 for Al atoms. This is not affected by the type of the charge balancing cations in the case of Si-O, while for the Al-O a slight variation has been observed (see Table III below). Moreover, other *ab initio* MD simulations as well as previously reported experiments [50,51] have shown that  $\text{Si}^{4+}$  is present in a tetrahedral coordination ( $\text{Si}_4$ ), which is in a good agreement with our simulations. Otherwise,  $\text{Al}^{3+}$  ions are present mostly in a fourfold coordinated  $\text{AlO}_4^-$  with a small fraction in the form of fivefold ( $\text{AlO}_5^{2-}$ ) and sixfold  $\text{AlO}_6^{3-}$  polyhedra as presented in Fig. 5. This is in good agreement with available experimental data [49,51].

The Si-Si, Al-Al, and Si-Al RDFs generally present the distance of separation between center of  $\text{SiO}_4$ - $\text{SiO}_4$ ,  $\text{AlO}_n$ - $\text{AlO}_n$ , and  $\text{SiO}_4$ - $\text{AlO}_n$  ( $n = 4, 5, 6$ ) polyhedra. These RDFs showed peaks around 3.2, 3.1, and 3.15 Å, respectively (see Supplemental Material Fig. S1 [52]). The cumulative coordination number  $N_{i-j}(r)$  of Si-Si, Al-Al, and Si-Al, have values around 1.75, 3.5, and 2.2 Å, respectively (see Supplemental Material Fig. S2 [52]). Hence, as it is well known in silica glass, each silicon tetrahedron is coordinated by four other tetrahedra. We

TABLE III. Short-range structural parameters of glasses obtained from molecular dynamics at 300 K. The cutoffs were set to 2.1 and 2.3 Å for the Si-O and Al-O pairs, and 2.66, 3.24, 3.8, 2.7, 3.1, 3.5, 4.0, and 2.6 Å for the Li-O, Na-O, K-O, Mg, Ca-O, Sr-O, Ba-O, and Zn-O pairs, respectively.

Glass systems	Si-O		Al-O		X-O	
	$r_{ij}$	$N_{ij}$	$r_{ij}$	$N_{ij}$	$r_{ij}$	$N_{ij}$
LiAS	1.61	4.02	1.73	4.05	1.99	4.02
NaAS	1.61	4.02	1.73	4.02	2.41	6.22
KAS	1.61	4.00	1.73	4.06	2.73	7.73
MgAS	1.61	3.99	1.73	4.12	2.03	4.79
CaAS	1.61	4.00	1.73	4.13	2.38	6.31
SrAS	1.61	4.00	1.73	4.10	2.59	8.19
BaAS	1.61	3.99	1.73	4.07	2.83	11.71
ZnAS	1.61	4.00	1.73	4.14	1.97	3.54

can notice that there are fewer silicon tetrahedra in the first coordination shell of a central one (1.75), while this number is higher for aluminum; this can be a result of the presence of  $\text{Al}^{IV}$  ( $n = 4, 5$ ) polyhedra in the glasses.

The bond angle distributions (BADs) can provide information about inter and intra polyhedral angles (linkage). The O-Si-O and O-Al-O BAD present the distribution of the angles inside  $\text{SiO}_4$  and  $\text{AlO}_4^-$  tetrahedra.

The bond angle distributions are presented in Fig. 6. For the O-Si-O distribution, no shift was reported as we changed the modifier, and this angle has been found to be centered around a mean value of  $109.1^\circ$  for all systems [Fig. 6(a)]. Moreover, we see that the O-Al-O BAD shifts to lower angles and becomes broader with increasing field strength [Fig. 6(b)]. In addition the intensity of the BAD decreases with increasing charge balancing cations field strength. The Si-O-Si and Al-O-Al bond angle distributions presented in Figs. 6(c) and 6(d) provide supplementary information on the linkage between the  $\text{SiO}_4$  tetrahedrons and  $\text{AlO}_4^-$  tetrahedra. We observe that Si-O-Si bond angle distribution has a value around  $147^\circ$  for all systems independently from the field strength of the charge balancing cations. On the other side, the Al-O-Al distribution has been shown to slightly depend on the type of the charge balancing cations. It presents a bimodal distribution with a first peak centered around  $120^\circ$  and another

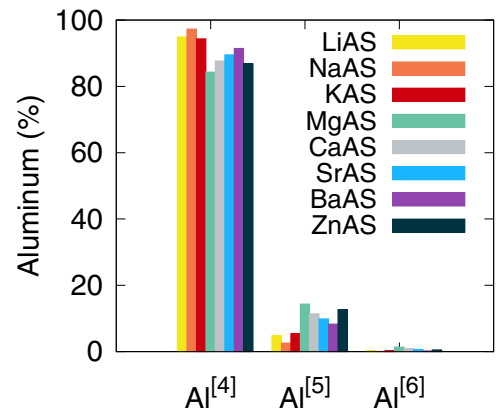


FIG. 5. Distribution of aluminum species in our systems at 300 K.

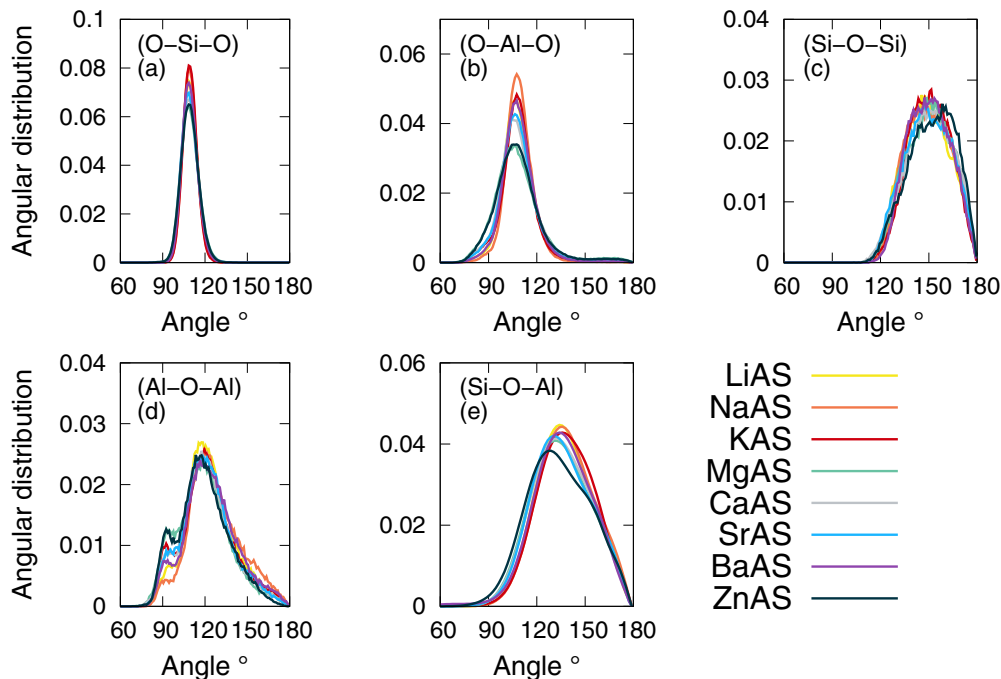


FIG. 6. Bond angles distributions obtained from MD simulations at 300 K. (a) O-Si-O, (b) O-Al-O, (c) Si-O-Si, (d) Al-O-Al, and (e) Si-O-Al.

around  $90^\circ$ . From the Al-O-Al ADF [Fig. 6(d)] and the Al coordination statistics in Fig. 5 we can suggest that the intense peak is attributed to the four-coordinated  $\text{AlO}_4^-$  tetrahedra while the secondary peak (the shoulder) is attributed mainly to  $\text{Al}^{[5]}$  polyhedra. We also notice that this second peak increases with the increasing amount of  $\text{Al}^{[5]}$  polyhedra with the highest intensity observed for MgAS and ZnAS and the lower intensity is observed for NaAS. This is in agreement with the high population of  $\text{Al}^{[5]}$  in MgAS and ZnAS and the low amount in NaAS. The Si-O-Al bond angle distributions shown in Fig. 6(e) represent the angle of the hybrid linkage between a  $\text{SiO}_4$  tetrahedra and an  $\text{AlO}_n$  polyhedra.

## 2. Oxygen local environment

The radial distribution function of the O-O pair is presented in Fig. 7(a), which shows that the mean length of the O-O bond (which is given by the first peak position) is not affected by the cations field strength (no shift of the RDF is observed) while the width of the first peak changes with FS. This suggests the presence of longer O-O bonds in the systems with higher field strength. This can be seen as an indication of the presence of larger polyhedral units in our systems with increasing FS.

The identification of the oxygen species is made according to the total number of bonds to Si and/or Al atoms. Thus,  $\text{O}^{[0]}$ ,  $\text{O}^{[1]}$ ,  $\text{O}^{[2]}$ ,  $\text{O}^{[3]}$ , and  $\text{O}^{[4]}$  stand for a free oxygen (FO), nonbridging oxygen (NBO), bridging oxygen (BO), oxygen tricluster (TBO) which is an oxygen linked to three network former atoms, and finally fourfold oxygen (FFO). As illustrated in Fig. 7(b), the population of FO and FFO is less than 0.3%. These small fractions of FO and FFO might be an artifact due to the high cooling rate used here and/or the

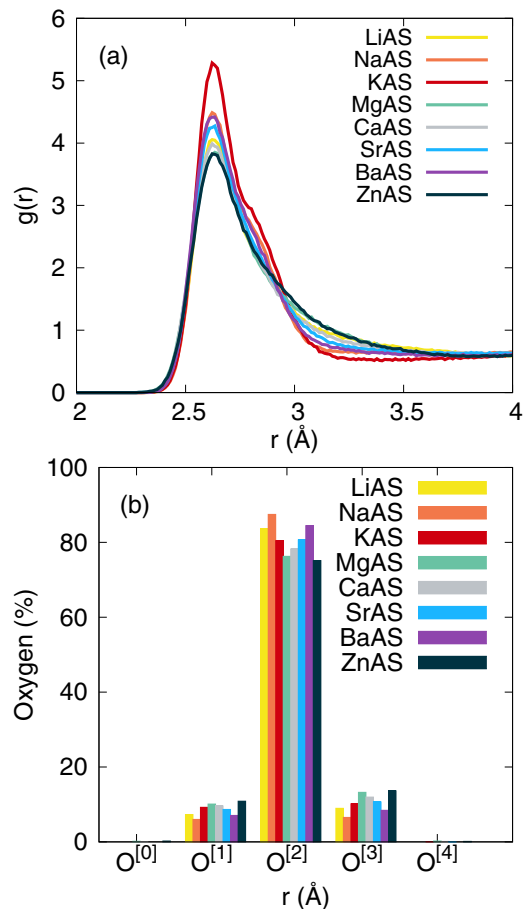


FIG. 7. O-O RDF (a) and the distribution of oxygen species (b) in our glasses at 300 K.

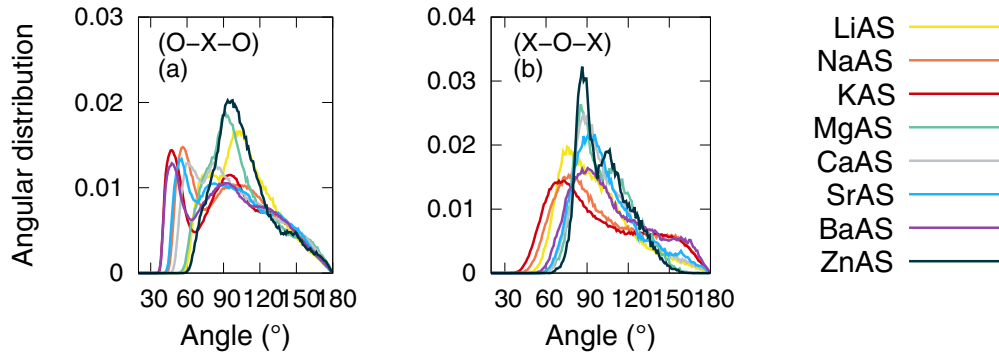


FIG. 8. Bond angle distributions obtained from MD simulations at 300 K: (a) O-X-O and (b) X-O-X where  $X = \text{Li, Na, K, Mg, Ca, Sr, Ba, and Zn}$ .

system size. Hence, the free oxygen and fourfold coordinated oxygen atoms are neglected in the further discussions.

Bridging oxygens have the highest population in the present charge balanced aluminosilicate glasses; this is rather normal since the present glasses are expected to mainly exhibit BOs and TBOs. However, we notice the existence of a non-negligible fraction of NBOs in all glasses (reaching 10%), which suggests that NBOs exist in aluminosilicate glasses with  $X_{n/2}^{n+}/\text{Al}_2\text{O}_3 = 1$  [53].

The effect of the charge balancing cations field strength is also present in the evolution of the oxygen species. If we focus only on the alkali aluminosilicate series, we can notice that LiAS, with the highest field strength, presents the highest NBO population; NaAS shows a high amount of BO while KAS has the highest number of TBO. In the alkaline earth aluminosilicate and ZnAS glasses, the highest field strength cations are Mg and Zn; they have the highest population of NBOs and TBOs. This suggests that as the field strength increases the population of BOs in the system decreases, while that of NBOs and TBOs increase [54].

### 3. Cations local environment

For the alkali charge balanced aluminosilicate glasses the Li-O, Na-O, and K-O RDFs have a maximum at 1.99, 2.41, and 2.73 Å (see Supplemental Material Figs. S1 and S2 [52]) showing that with increasing field strength the cation oxygen bond length decreases. Furthermore, the coordination number seems also to decrease with decreasing field strength. The alkaline earth and ZnO aluminosilicate glasses illustrate a similar behavior as seen in alkali aluminosilicate glasses for both X-O bond lengths and coordination numbers; the bond length and the coordination number is increasing as  $\text{Zn} < \text{Mg} < \text{Ca} < \text{Sr} < \text{Ba}$ .

To get more insight into the local environment of the charge balancing cations, we did compute and plot the RDF and cumulative coordination functions of these cations with Si and Al (see Supplemental Material Figs. S1 and S2 [52]). We observe a negative correlation between FS and Si-X, Al-X lengths; this effect is also observed in the coordination numbers of Si-X and Al-X. The X-X RDF shows that the X-X distance decreases with increasing FS, which can be attributed to the change in the X-O-X BAD linkage. Now, if we look at the BAD of O-X-O and X-O-X as plotted in

Figs. 8(a) and 8(b), we can notice that the environment of the charge balancing cation is more complex. This is due to the high coordination states that can be attained by these cations presenting a maximum of 12 for Ba cations and a minimum of 3.5 for the Zn cations. For lower FS cations, O-X-O BAD shows a bimodal distribution and as the FS increases it becomes a unimodal distribution with angle values centered around  $109^\circ$ , which is also in accordance with the evolution of the coordination number of those cations. For X-O-X BAD, the same behavior is noticed and the BAD is wider for lower cations field strength and becomes more localized around  $90^\circ$  for high FS cations.

## IV. DISCUSSION

In the present study, we investigate the structural change in aluminosilicate glasses due to different charge balancing cations. Our results showed that the elastic moduli (Fig. 2) are in good agreement with the experimental data measured by Brillouin light scattering [2]. Otherwise, the glass transition temperature  $T_g$  is higher than the experimental values, which we attribute to the high cooling rate used in MD simulations and probably to the interatomic potential that was not fitted on this property. It is also worth stressing that the calculation of the glass transition temperature values is sensitive to the system size and cooling rate. Nevertheless, we noticed a striking similar behavior between MD  $T_g$  values and those obtained experimentally. This suggests that the behavior of  $T_g$  versus the FS is a real effect observed in the present work and is not an artifact generated by MD simulations. Indeed, the values of  $T_g$  and other glass properties can be affected by the cooling rate used in the quenching process. However, in the current study we used several cooling rates for knowing  $1.10^{13}$ ,  $5.10^{12}$ ,  $1.10^{12}$ , and  $5.10^{11}$  K/ps and we didn't see any noticeable difference that will affect our conclusions. The mechanical properties were slightly affected by the cooling rate while  $T_g$  decreased with decreasing cooling rate which is a normal effect as the system was allowed to relax more in lower cooling rates, thus, more local minima were explored and the final glass is found in a relatively more stable state compared with the glasses produced using higher cooling rates. The bond lengths in our glasses were not affected by the cooling rates neither the coordination numbers of the glass formers (Si and Al) which is in accordance with previous



studies on the cooling rate effect in oxide glasses [35,36,55–57]. A discussion of the cooling rate effect on the glass properties in oxide and metallic glasses can be found in the Supplemental Material [52]; see also Refs. [25,35,36,55–68] for further details.

In order to get a better understanding of the effect of different charge balancing cations on the physical properties of aluminosilicate glasses, we can correlate the structural change with the elastic moduli and the glass transition temperature. Indeed, the elastic moduli give us information about the stiffness of the glass with respect to deformation, which obviously reflects the bond strength. However, the elastic moduli do not depend only on the bond strength but also on the coordination, the degree of glass network polymerization, atomic packing density, and in some cases on the medium-range order of the glass as highlighted by Rouxel [69]. Rouxel did put some light on the relationships between the elastic moduli and the atomic network organization.

When we doped the aluminosilicate glasses with different charge balancing cations we did not observe any noticeable change in the mean bond lengths of Si-O, Al-O, and O-O pairs; this is seen through the unchanged position of the RDF first peak. However, the intensity of this first peak which describes the density variation in the first coordination shell does change as a function of the field strength. Higher charge balancing field strength leads to lower intensity of the Si-O and Al-O RDFs first peak as seen in Figs. 4(a) and 4(b). This effect is due to the ability of cations with high field strength to form stronger and thus shorter bonds with oxygen atoms compared to cations with low field strength. This could also be the reason for the increase observed in the evolution of the elastic moduli with the FS, as the Young's and shear moduli represent the stiffness of a material subjected to a uniaxial load and shear loading, respectively. High elastic moduli mean a high resistance to elastic deformation for a given load. This behavior is strongly dependent on the bond strength as has been suggested by Makishima and Mackenzie [70]. This suggests that the elastic moduli increase with decreasing molar volume or inversely with the atomic density. In the present work, this effect is clearly seen in bulk modulus, while it is also noticed for shear and Young's moduli (see Supplemental Material Fig. S3 [52]). The Poisson's ratio ( $\nu$ ) is an important parameter to understand the mechanical behavior of glasses [71]. It is a measure of the resistance of a material to volume change with respect to shape change [69]. As presented previously (Fig. 2), Poisson's ratio doesn't depend on the field strength of the charge balancing cations. If we take a look at the evolution of  $\nu$  as a function of the molar volume it is clearly seen that there are three distributions of Poisson's ratio (see Supplemental Material Fig. S4 [52]). This suggests that in aluminosilicate glasses  $\nu$  depends on the family of the nonframework oxide rather than on the value of the field strength. In addition to that, the present MD simulations show that the Poisson's ratio generally decreases as a function of the molar volume, which has been also observed in BLS experiments [2]. This can be explained by the fact that glasses with lower molar volume have a closely packed structure which is supposed to exhibit small volume changes when changing shape, due to the limited space for densification. Though this explanation is generally applicable to our glasses,

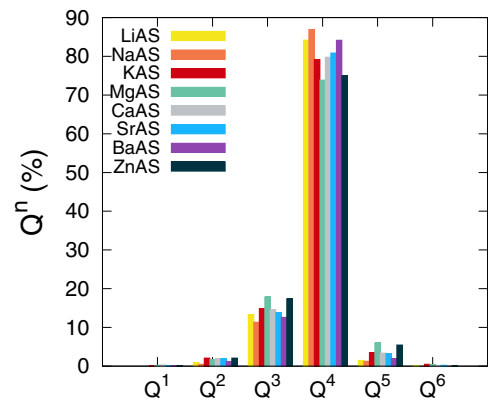


FIG. 9.  $Q^n$  distribution of network formers (Si and Al atoms) in the glasses  $(X_{n/2}^{n+}O - Al_2O_3) - SiO_2$  where  $(X = Li, Na, K, Mg, Ca, Sr, Ba, \text{ and } Zn)$  obtained from MD simulations at 300 K.

there is some fluctuation in the values as seen in both alkali, alkaline earth, and ZnO aluminosilicate glasses; this can be attributed to the connectivity of the network as glasses with higher connectivity are more rigid and show more resistance to elastic deformation [71]. To argue with this, we performed a statistical analysis of the  $Q^n$  (i.e., the distribution of BOs in each silicon and aluminum polyhedron, and  $n$  is the number of BOs per polyhedron.) distribution in our glasses, presented in Fig. 9. As expected, the highest population is that of  $Q^4$  since the glasses are supposed to be fully connected. For high field strength charge balancing cations, there is a tendency to form more  $Q^3$  and  $Q^2$  species than the low charge balancing cations FS.

The glass transition temperature  $T_g$  also presents a dependence on the charge balancing cations field strength, as seen previously in Fig. 3.  $T_g$  decreases with increasing FS, which can be attributed to the modification of the aluminosilicate glasses structure mainly in the Si and/or Al environment and to the change in oxygen species due to the presence of alkali, alkaline earth, and Zn elements. As indicated before, in the present charge balanced aluminosilicate glasses, all silicon atoms are four-coordinated with oxygen atoms. As illustrated in Fig. 5, aluminum atoms are primarily found in fourfold coordinated species, while there exist some five-coordinated Al, which leads to the formation of  $Q^{[5]}$ . We note also the existence of a negligible amount of  $Al^{[6]}$  which we preferred to ignore in our analysis due to its minor contribution. The abundance of each state depends on the type and the field strength of the charge balancing cations. For the alkali aluminosilicate glasses, in the NaAS system there are more  $Al^{[4]}$  than in the LiAS and KAS systems, and in the KAS system there are more  $Al^{[5]}$ . Moreover, for oxygen species, which can be seen as an indication of the network connectivity, more BOs suggest a more connected glass network. Figure 7(b) shows that more BOs are present in NaAS glass than in the other aluminosilicate glasses, while ZnAS glass presents the largest number of TBOs.

The energetic environment of silicon atoms is supposed to be unaffected by the type and/or the size of the charge balancing cations; this assumption is based on the fourfold coordinated silicon atoms, the unchanged mean Si-O bond

length, and intratetrahedral angles O-Si-O found in our simulations (see Supplemental Material Fig. S5 [(a) and (b)] [52]). Additionally, for alkali aluminosilicate glasses the environment of Al atoms is also not affected by the charge balancing cations FS, while for alkaline earth and ZnO aluminosilicate glasses a shift toward higher values of the potential energy is observed with increasing FS (see Supplemental Material Fig. S5 [(c) and (d)] [52]). This is in full agreement with the change in the  $\text{Al}^{[n]}$  population and also the Al coordination number as summarized in Table III. Furthermore, we can characterize the oxygen environment energetically, by providing the per-atom potential energy for each specie. For alkali aluminosilicate, we found a bimodal distribution and no dependence on the FS has been noticed. Lower energy values correspond to TBOs and BOs, while NBOs have higher potential energy. On the other hand, in alkaline earth and ZnO aluminosilicate, a dependence on the cations FS was observed as there is a shift toward lower energy values. This is in agreement with the oxygen statistics given in Fig. 7(b) in which there is a tendency to have more TBOs in higher FS aluminosilicate (see Supplemental Material Fig. S5 [(e) and (f)] [52]). The difference in FS (ionic radius) affects the number of oxygen atoms that can be present around the charge balancing cations (see Table III). Hence, fewer oxygen atoms

can be present around high field strength cations (small ionic radius), which causes each oxygen to have more concentrated negative charge in order to balance the cations charge. This could also explain why this effect is more pronounced for divalent cations and not for monovalent cations. However, smaller divalent cations need to have a more negative average residual charge, suggesting that the larger cations can charge balance the negative charges on the Si-O-Al bridging oxygens. This is supported by the aluminum statistics as presented in Fig. 5 and the results reported previously by Smedskejaer *et al.* in their experimental study of the effect of ZnO on the structure of sodium aluminosilicate glasses [72]. Consequently, higher field strength charge balancing cations promote the concentration of negative charges on their local NBOs, which causes conversion of  $\text{Al}^{[4]}$  to  $\text{Al}^{[5]}$ .

From the distribution of potential energy per atom of the charge balancing cations given in Figs. 10(a) and 10(b), we can notice that cations with similar FS have similar environment and that high FS cations can have stronger X-O bonds. This in fact is in good accordance with the coordination number distribution and the cations size, as large cations have a bigger surface to distribute the charge which can result in high coordination number, which has an effect on the charge balancing capability of each cation. This suggests that high field strength charge balancing cations such as Mg and Zn can be considered as intermediate oxides or pseudonetwork formers rather than network modifier. This was also suggested

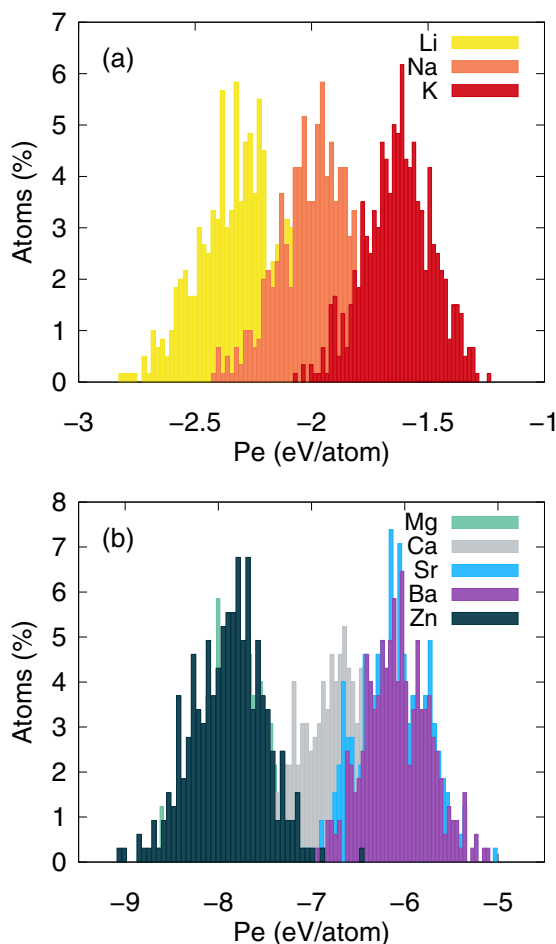


FIG. 10. Potential energy per atom distribution of (a) (Li, Na, and K) and (b) (Mg, Ca, Sr, Ba, and Zn) obtained from MD simulations at 300 K.

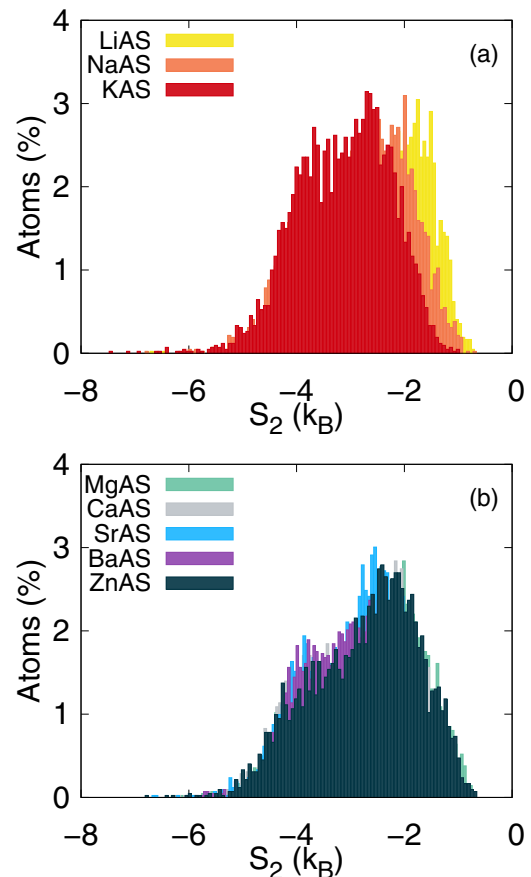


FIG. 11. Distribution of  $S_2$  in our glasses at 300 K, (a) alkali aluminosilicate and (b) alkaline earth and Zn aluminosilicate.

by Desirena *et al.* and Smedskjaer *et al.* for different glasses [72,73]. Besides, this also can be the reason of the high elastic moduli reported herein for MgAS and ZnAS glasses.

Additionally, it is also possible to quantify the local configurational entropy or entropy fingerprint using two-body correlation functions as described in Sec. 2. As a matter of fact, there are many different definitions of configurational entropy which is mainly due to the difficulty in the computation of the vibrational contributions, a useful approximation which accounts for about 90% of the configurational entropy can be used for simple liquids, which requires only the pair correlation function [39,74,75]. The entropy fingerprint distribution is presented in Figs. 11(a) and 11(b). In the glasses containing high field strength charge balancing cations, there is a trend showing that these systems are more disordered than those containing low charge balancing cation FS. This effect can be explained by X-O bond strength ( $X = \text{Li, Na, K, Mg, Ca, Sr, Ba, and Zn}$ ). The X-O bond strength is correlated positively with FS, giving evidence that for low FS cations there is less competition between X, Si, and Al to form bonds with oxygen atoms, resulting in a low configurational entropy of the system. For alkaline earth cations and Zn this effect is not clear but we noticed a shift to higher values of  $S_2$  with increasing field strength.

## V. CONCLUSION

We used MD simulations to study the effect of charge balancing cations on the structural and physical properties of aluminosilicate glasses with the composition  $(X_{n/2}^{n+}O - Al_2O_3)_{50} - (SiO_2)_{50}$  where X is Li, Na, K, Mg, Ca, Sr, Ba, and Zn. The ratio  $R = \frac{X_{n/2}^{n+}O}{Al_2O_3}$  was set to 1.

Elastic properties were investigated using the energy minimization and compared to experiments. The glass transition temperature and elastic properties are found to strongly depend on the charge balancing cations type and field strength. Our results are in a realistic agreement with available experimental data measured by BLS experiments. In addition, the charge balancing cations FS have been found to induce a structural change manifested by the change in NBOs, BOs, TBOs, and  $Al^{[IV]}$  populations, without neglecting its effect on the Al-O-Al BAD and the  $Q^n$  distribution. The results suggest that the smaller cations (high FS) (e.g., Mg and Zn) behave more like network formers than network modifiers as indicated by the coordination numbers and bond angle distributions, while the larger ones (low FS) behave more as network modifiers. This explains the increase of the elastic moduli as a function of charge balancing cations field strength. Moreover, cations with similar FS behave similarly as has been seen for MgO and ZnO aluminosilicate glasses, although they have different electronic configurations. The insights obtained from the present molecular dynamics simulations to explain experimental results will help in understanding the effect of charge balancing cations on the observed glass properties and in designing glass compositions for more advanced technological applications.

## ACKNOWLEDGMENTS

A.A thanks Z. Xie for fruitful discussions and Prof. Dr.-Ing. Erik Bitzek for providing the computational resources. Computing resources were provided by the Regionale RechenZentrum Erlangen (RRZE).

- 
- [1] J. Rösler, H. Harders, and M. Bäker, in *Mechanical Behavior of Engineering Materials: Metals, Ceramics, Polymers, and Composites* (Springer, Berlin, 2007), p. 534.
  - [2] C. Weigel, C. Le Losq, R. Violla, C. Dupas, S. Clément, D. R. Neuville, and B. Rufflé, Elastic moduli of XAlSiO4 aluminosilicate glasses: Effects of charge-balancing cations, *J. Non-Cryst. Solids* **447**, 267 (2016).
  - [3] J. Luo, J. Wang, E. Bitzek, J. Y. Huang, H. Zheng, L. Tong, Q. Yang, J. Li, and S. X. Mao, Size-dependent brittle-to-ductile transition in silica glass nanofibers, *Nano Lett.* **16**, 105 (2016).
  - [4] F. Lechenault, C. L. Rountree, F. Cousin, J. P. Bouchaud, L. Ponson, and E. Bouchaud, Damage of silicate glasses during stress corrosion, *J. Phys.: Conf. Ser.* **319**, 012005 (2011).
  - [5] R. Belli, M. Wendler, M. R. Cicconi, D. de Ligny, A. Petschelt, K. Werbach, H. Peterlik, and U. Lohbauer, Fracture anisotropy in texturized lithium disilicate glass-ceramics, *J. Non-Cryst. Solids* **481**, 457 (2018).
  - [6] Y. Yu, M. Wang, N. M. Anoop Krishnan, M. M. Smedskjaer, K. Deenamma Vargheese, J. C. Mauro, M. Balonis, and M. Bauchy, Hardness of silicate glasses: Atomic-scale origin of the mixed modifier effect, *J. Non-Cryst. Solids* **489**, 16 (2018).
  - [7] A. Mohajerani, V. Martin, D. Boyd, and J. W. Zwanziger, On the mechanical properties of lead borate glass, *J. Non-Cryst. Solids* **381**, 29 (2013).
  - [8] R. Limbach, A. Winterstein-Beckmann, J. Dellith, D. Möncke, and L. Wondraczek, Plasticity, crack initiation and defect resistance in alkali-borosilicate glasses: From normal to anomalous behavior, *J. Non-Cryst. Solids* **417-418**, 15 (2015).
  - [9] V. M. Sglavo, E. Mura, D. Milanese, and J. Lousteau, Mechanical properties of phosphate glass optical fibers, *Int. J. Appl. Glas. Sci.* **5**, 57 (2014).
  - [10] N. Sharmin, A. J. Parsons, C. D. Rudd, and I. Ahmed, Effect of boron oxide addition on fibre drawing, mechanical properties and dissolution behavior of phosphate-based glass fibres with fixed 40, 45 and 50 mol% P<sub>2</sub>O<sub>5</sub>, *J. Biomater. Appl.* **29**, 639 (2014).
  - [11] W. Wang, R. Christensen, B. Curtis, S. W. Martin, and J. Kieffer, A new model linking elastic properties and ionic conductivity of mixed network former glasses, *Phys. Chem. Chem. Phys.* **20**, 1629 (2018).
  - [12] M. Storek, M. Adjei-Acheamfour, R. Christensen, S. W. Martin, and R. Böhmer, Positive and negative mixed glass former effects in sodium borosilicate and borophosphate glasses studied by <sup>23</sup>Na NMR, *J. Phys. Chem. B* **120**, 4482 (2016).
  - [13] M. Bauchy, Structural, vibrational, and elastic properties of a calcium aluminosilicate glass from molecular dynamics simulations: The role of the potential, *J. Chem. Phys.* **141**, 024507 (2014).

- [14] M. Dittmer, C. F. Yamamoto, C. Bocker, and C. Rüssel, Crystallization and mechanical properties of MgO/Al<sub>2</sub>O<sub>3</sub>/SiO<sub>2</sub>/ZrO<sub>2</sub> glass-ceramics with and without the addition of yttria, *Solid State Sci.* **13**, 2146 (2011).
- [15] Y. Xiang, J. Du, M. M. Smedskjaer, and J. C. Mauro, Structure and properties of sodium aluminosilicate glasses from molecular dynamics simulations, *J. Chem. Phys.* **139**, 044507 (2013).
- [16] A. Pönitzsch, M. Nofz, L. Wondraczek, and J. Deubener, Bulk elastic properties, hardness and fatigue of calcium aluminosilicate glasses in the intermediate-silica range, *J. Non-Cryst. Solids* **434**, 1 (2016).
- [17] B. O. Mysen, Role of Al in depolymerized, peralkaline aluminosilicate melts in the systems Li<sub>2</sub>O-Al<sub>2</sub>O<sub>3</sub>-SiO<sub>2</sub>, Na<sub>2</sub>O-Al<sub>2</sub>O<sub>3</sub>-SiO<sub>2</sub> and K<sub>2</sub>O-Al<sub>2</sub>O<sub>3</sub>-SiO<sub>2</sub>, *Am. Mineral.* **75**, 120 (1990).
- [18] K. E. Kelsey, J. F. Stebbins, D. M. Singer, G. E. Brown, J. L. Mosenfelder, and P. D. Asimow, Cation field strength effects on high pressure aluminosilicate glass structure: Multinuclear NMR and La XAFS results, *Geochim. Cosmochim. Ac.* **73**, 3914 (2009).
- [19] J. R. Allwardt, J. F. Stebbins, B. C. Schmidt, D. J. Frost, A. C. Withers, and M. M. Hirschmann, Aluminum coordination and the densification of high-pressure aluminosilicate glasses, *Am. Mineral.* **90**, 1218 (2005).
- [20] K. E. Kelsey, J. R. Allwardt, and J. F. Stebbins, Ca–Mg mixing in aluminosilicate glasses: An investigation using <sup>17</sup>O MAS and 3QMAS and <sup>27</sup>Al MAS NMR, *J. Non-Cryst. Solids* **354**, 4644 (2008).
- [21] A. Atila, E. M. Ghardi, A. Hasnaoui, and S. Ouaskit, Alumina effect on the structure and properties of calcium aluminosilicate in the percalcic region: A molecular dynamics investigation, *J. Non-Cryst. Solids* **525**, 119470 (2019).
- [22] E. M. Ghardi, A. Atila, M. Badawi, A. Hasnaoui, and S. Ouaskit, Computational insights into the structure of barium titanosilicate glasses, *J. Am. Ceram. Soc.* **102**, 6626 (2019).
- [23] Z. Liu, Y. Hu, X. Li, W. Song, S. Goyal, M. Micoulaut, and M. Bauchy, Glass relaxation and hysteresis of the glass transition by molecular dynamics simulations, *Phys. Rev. B* **98**, 104205 (2018).
- [24] B. Mantisi, M. Bauchy, and M. Micoulaut, Cycling through the glass transition: Evidence for reversibility windows and dynamic anomalies, *Phys. Rev. B* **92**, 134201 (2015).
- [25] M. Kbirou, M. Mazroui, and A. Hasnaoui, Atomic packing and fractal behavior of Al-Co metallic glasses, *J. Alloys Compd.* **735**, 464 (2018).
- [26] A. Hasnaoui, H. Van Swygenhoven, and P. M. Derlet, Dimples on nanocrystalline fracture surfaces as evidence for shear plane formation, *Science* **300**, 1550 (2003).
- [27] H. Van Swygenhoven, P. M. Derlet, and A. Hasnaoui, Atomic mechanism for dislocation emission from nanosized grain boundaries, *Phys. Rev. B* **66**, 024101 (2002).
- [28] A. Hasnaoui, H. Van Swygenhoven, and P. M. Derlet, Cooperative processes during plastic deformation in nanocrystalline fcc metals: A molecular dynamics simulation, *Phys. Rev. B* **66**, 184112 (2002).
- [29] A. Pedone, G. Malavasi, M. C. Menziani, A. N. Cormack, and U. Segre, A new self-consistent empirical interatomic potential model for oxides, silicates, and silicas-based glasses, *J. Phys. Chem. B* **110**, 11780 (2006).
- [30] A. Pedone, G. Malavasi, M. Cristina Menziani, U. Segre, and A. N. Cormack, Molecular dynamics studies of stress-strain behavior of silica glass under a tensile load, *Chem. Mater.* **20**, 4356 (2008).
- [31] J. Turlier, S. Chaussedent, P. Raso, X. Bidault, M. Vermillac, A. Mehdi, D. Neuville, W. Blanc, N. Gaumer, D. Guichaoua, and H. Fneich, Molecular dynamics study of rare-earth doped Mg-silicate nanoparticles in vitreous silica: From the preform to the fiber, in *Fiber Lasers Glas. Photonics Mater. through Appl.*, edited by S. Taccheo, M. Ferrari, and J. I. Mackenzie (SPIE, Bellingham, 2018), Vol. 10683, p. 103.
- [32] J. Luo, K. D. Vargheese, A. Tandia, G. Hu, and J. C. Mauro, Crack nucleation criterion and its application to impact indentation in glasses, *Sci. Rep.* **6**, 23720 (2016).
- [33] S. Plimpton, Fast parallel algorithms for short-range molecular dynamics, *J. Comput. Phys.* **117**, 1 (1995).
- [34] A. Stukowski, Visualization and analysis of atomistic simulation data with OVITO—the open visualization tool, *Model. Simul. Mater. Sci. Eng.* **18**, 015012 (2010).
- [35] A. Tilocca, Cooling rate and size effects on the medium-range structure of multicomponent oxide glasses simulated by molecular dynamics, *J. Chem. Phys.* **139**, 114501 (2013).
- [36] X. Li, W. Song, K. Yang, N. M. A. Krishnan, B. Wang, M. M. Smedskjaer, J. C. Mauro, G. Sant, M. Balonis, and M. Bauchy, Cooling rate effects in sodium silicate glasses: Bridging the gap between molecular dynamics simulations and experiments, *J. Chem. Phys.* **147**, 074501 (2017).
- [37] J. Ding, G. Pan, L. Du, J. Lu, W. Wang, X. Wei, and J. Li, Molecular dynamics simulations of the local structures and transport properties of Na<sub>2</sub>CO<sub>3</sub> and K<sub>2</sub>CO<sub>3</sub>, *Appl. Energy* **227**, 555 (2018).
- [38] R. E. Nettleton and M. S. Green, Expression in terms of molecular distribution functions for the entropy density in an infinite system, *J. Chem. Phys.* **29**, 1365 (1958).
- [39] P. M. Piaggi and M. Parrinello, Entropy based fingerprint for local crystalline order, *J. Chem. Phys.* **147**, 114112 (2017).
- [40] A. Baranyai and D. J. Evans, Direct entropy calculation from computer simulation of liquids, *Phys. Rev. A* **40**, 3817 (1989).
- [41] T. Morita and K. Hiroike, A new approach to the theory of classical fluids. III: General treatment of classical systems, *Prog. Theor. Phys.* **25**, 537 (1961).
- [42] S. Prestipino and P. V. Giaquinta, The entropy multiparticle-correlation expansion for a mixture of spherical and elongated particles, *J. Stat. Mech.* (2004) P09008.
- [43] M. Bauchy and M. Micoulaut, Atomic scale foundation of temperature-dependent bonding constraints in network glasses and liquids, *J. Non-Cryst. Solids* **357**, 2530 (2011).
- [44] J. E. Shelby, in *Introduction to Glass Science and Technology* (The Royal Society of Chemistry, Cambridge, 2005), pp. X001–X004.
- [45] J. Ketkaew, W. Chen, H. Wang, A. Datye, M. Fan, G. Pereira, U. D. Schwarz, Z. Liu, R. Yamada, W. Dmowski, M. D. Shattuck, C. S. O'Hern, T. Egami, E. Bouchbinder, and J. Schroers, Mechanical glass transition revealed by the fracture toughness of metallic glasses, *Nat. Commun.* **9**, 3271 (2018).
- [46] C. Romano, B. Poe, V. Mincione, K. U. Hess, and D. B. Dingwell, The viscosities of dry and hydrous XAlSi<sub>3</sub>O<sub>8</sub> (X=Li, Na, K, Ca<sub>0.5</sub>, Mg<sub>0.5</sub>) melts, *Chem. Geol.* **174**, 115 (2001).

- [47] A. Navrotsky, K. L. Geisinger, P. McMillan, and G. V. Gibbs, The tetrahedral framework in glasses and melts—inferences from molecular orbital calculations and implications for structure, thermodynamics, and physical properties, *Phys. Chem. Miner.* **11**, 284 (1985).
- [48] J. R. Allwardt, B. T. Poe, and J. F. Stebbins, The effect of fictive temperature on Al coordination in high-pressure (10 GPa) sodium aluminosilicate glasses, *Am. Mineral.* **90**, 1453 (2005).
- [49] T. Charpentier, K. Okhotnikov, A. N. Novikov, L. Hennem, H. E. Fischer, D. R. Neuville, and P. Florian, Structure of strontium aluminosilicate glasses from molecular dynamics simulation, neutron diffraction, and nuclear magnetic resonance studies, *J. Phys. Chem. B* **122**, 9567 (2018).
- [50] T. Ohkubo, E. Tsuchida, K. Deguchi, S. Ohki, T. Shimizu, T. Otomo, and Y. Iwadate, Insights from ab initio molecular dynamics simulations for a multicomponent oxide glass, *J. Am. Ceram. Soc.* **101**, 1122 (2018).
- [51] M. Ren, J. Y. Cheng, S. P. Jaccani, S. Kapoor, R. E. Youngman, L. Huang, J. Du, and A. Goel, Composition-structure-property relationships in alkali aluminosilicate glasses: A combined experimental-computational approach towards designing functional glasses, *J. Non-Cryst. Solids* **505**, 144 (2019).
- [52] See Supplemental Material at <http://link.aps.org/supplemental/10.1103/PhysRevB.100.144109> for a discussion about the cooling rate effect and more structural details.
- [53] L. M. Thompson and J. F. Stebbins, Non-stoichiometric non-bridging oxygens and five-coordinated aluminum in alkaline earth aluminosilicate glasses: Effect of modifier cation size, *J. Non-Cryst. Solids* **358**, 1783 (2012).
- [54] K. F. Frederiksen, K. Januchta, N. Mascaraque, R. E. Youngman, M. Bauchy, S. J. Rzoska, M. Bockowski, and M. M. Smedskjaer, Structural compromise between high hardness and crack resistance in aluminoborate glasses, *J. Phys. Chem. B* **122**, 6287 (2018).
- [55] P. Bhaskar, Y. Maurya, R. Kumar, R. Ravinder, A. R. Allu, S. Das, N. N. Gosvami, R. E. Youngman, M. S. Bødker, N. Mascaraque, M. M. Smedskjaer, M. Bauchy, and N. M. A. Krishnan, Cooling rate effects on the structure of 45s5 bioglass: Computational and experimental evidence of si-p avoidance, [arXiv:1906.10111](https://arxiv.org/abs/1906.10111).
- [56] J. M. D. Lane, Cooling rate and stress relaxation in silica melts and glasses via microsecond molecular dynamics, *Phys. Rev. E* **92**, 012320 (2015).
- [57] N. M. A. Krishnan, B. Wang, Y. Yu, Y. Le Pape, G. Sant, and M. Bauchy, Enthalpy Landscape Dictates the Irradiation-Induced Disorder of Quartz, *Phys. Rev. X* **7**, 031019 (2017).
- [58] M. Kbirou, S. Trady, A. Hasnaoui, and M. Mazroui, Cooling rate dependence and local structure in aluminum monatomic metallic glass, *Philos. Mag.* **97**, 2753 (2017).
- [59] S. Trady, M. Mazroui, A. Hasnaoui, and K. Saadouni, Molecular dynamics study of atomic-level structure in monatomic metallic glass, *J. Non-Cryst. Solids* **443**, 136 (2016).
- [60] S. Trady, A. Hasnaoui, M. Mazroui, and K. Saadouni, Local atomic structures of single-component metallic glasses, *Eur. Phys. J. B* **89**, 223 (2016).
- [61] M. Jafary-Zadeh, R. Tavakoli, J. Koh, Z. Aitken, and Y.-W. Zhang, Effect of chemical composition and affinity on the short- and medium-range order structures and mechanical properties of Zr-Ni-Al metallic glass, *J. Non-Cryst. Solids* **456**, 68 (2017).
- [62] S. C. Chowdhury, B. Z. G. Haque, and J. W. Gillespie, Molecular dynamics simulations of the structure and mechanical properties of silica glass using ReaxFF, *J. Mater. Sci.* **51**, 10139 (2016).
- [63] R. Ravinder, R. Kumar, M. Agarwal, and N. M. A. Krishnan, Evidence of a two-dimensional glass transition in graphene: Insights from molecular simulations, *Sci. Rep.* **9**, 4517 (2019).
- [64] K. Vollmayr, W. Kob, and K. Binder, How do the properties of a glass depend on the cooling rate: A computer simulation study of a Lennard-Jones system, *J. Chem. Phys.* **105**, 4714 (1996).
- [65] H. Shintani and H. Tanaka, Frustration on the way to crystallization in glass, *Nat. Phys.* **2**, 200 (2006).
- [66] L. Deng and J. Du, Effects of system size and cooling rate on the structure and properties of sodium borosilicate glasses from molecular dynamics simulations, *J. Chem. Phys.* **148**, 024504 (2018).
- [67] J. Buchholz, W. Paul, F. Varnik, and K. Binder, Cooling rate dependence of the glass transition temperature of polymer melts: Molecular dynamics study, *J. Chem. Phys.* **117**, 7364 (2002).
- [68] J. Tan, S. Zhao, W. Wang, G. Davies, and X. Mo, The effect of cooling rate on the structure of sodium silicate glass, *Mater. Sci. Eng.: B* **106**, 295 (2004).
- [69] T. Rouxel, Elastic properties and short-to medium-range order in glasses, *J. Am. Ceram. Soc.* **90**, 3019 (2007).
- [70] A. Makishima and J. Mackenzie, Direct calculation of Young's modulus of glass, *J. Non-Cryst. Solids* **12**, 35 (1973).
- [71] K. Januchta, M. Bauchy, R. E. Youngman, S. J. Rzoska, M. Bockowski, and M. M. Smedskjaer, Modifier field strength effects on densification behavior and mechanical properties of alkali aluminoborate glasses, *Phys. Rev. Mater.* **1**, 063603 (2017).
- [72] M. M. Smedskjaer, R. E. Youngman, and J. C. Mauro, Impact of ZnO on the structure and properties of sodium aluminosilicate glasses: Comparison with alkaline earth oxides, *J. Non-Cryst. Solids* **381**, 58 (2013).
- [73] H. Desirena, A. Schülzgen, S. Sabet, G. Ramos-Ortiz, E. de la Rosa, and N. Peyghambarian, Effect of alkali metal oxides R<sub>2</sub>O (R = Li, Na, K, Rb and Cs) and network intermediate MO (M = Zn, Mg, Ba and Pb) in tellurite glasses, *Opt. Mater.* **31**, 784 (2009).
- [74] A. Banerjee, S. Sengupta, S. Sastry, and S. M. Bhattacharyya, Role of Structure and Entropy in Determining Differences in Dynamics for Glass Formers with Different Interaction Potentials, *Phys. Rev. Lett.* **113**, 225701 (2014).
- [75] J. E. Hallett, F. Turci, and C. P. Royall, Local structure in deeply supercooled liquids exhibits growing length scales and dynamical correlations, *Nat. Commun.* **9**, 3272 (2018).